HAL
open science

Impact of defects on Auger recombination in c -plane InGaN/GaN single quantum well in the efficiency droop regime

W. Liu, C. Haller, Y. Chen, T. Weatherley, J.-F. Carlin, Gwenolé Jacopin, R. Butté, N. Grandjean

To cite this version:

W. Liu, C. Haller, Y. Chen, T. Weatherley, J.-F. Carlin, et al.. Impact of defects on Auger recombination in c -plane InGaN/GaN single quantum well in the efficiency droop regime. Applied Physics Letters, 2020, 116 (22), pp.222106. 10.1063/5.0004321 . hal-03043417

HAL Id: hal-03043417

https://hal.science/hal-03043417v1

Submitted on 18 Dec 2020

HAL is a multi-disciplinary open access archive for the deposit and dissemination of scientific research documents, whether they are published or not. The documents may come from teaching and research institutions in France or abroad, or from public or private research centers.

L'archive ouverte pluridisciplinaire **HAL**, est destinée au dépôt et à la diffusion de documents scientifiques de niveau recherche, publiés ou non, émanant des établissements d'enseignement et de recherche français ou étrangers, des laboratoires publics ou privés.

Impact of point defects on Auger recombination in c-plane InGaN/GaN single quantum well in the efficiency droop regime

W. Liu,[1] C. Haller,[1] Y. Chen,[1] T. Weatherley,[1] J.-F. Carlin,[1] G. Jacopin,[1, a)] R. Butté,[1, b)] and N. Grandjean[1]
Institute of Physics, École Polytechnique Fédérale de Lausanne (EPFL), CH-1015 Lausanne, Switzerland

(Dated: 11 February 2020)

We study the impact of non-radiative point defects (PDs) on Auger recombination in c-plane InGaN/GaN single quantum well (SQW) in the efficiency droop regime using high injection time-resolved photoluminescence. The PD density in the SQW is controlled by tuning the thickness of an InAlN underlayer. When the PD density is increased, apart from Shockley-Read-Hall (SRH) and standard Auger recombination, introducing an extra defect-assisted Auger process is required to reconcile the discrepancy observed between the usual ABC model and experimental data. We derive a linear dependence between the SRH coefficient and the bimolecular defect-assisted Auger coefficient, which suggests that the generated PDs can behave as scattering centers responsible for indirect Auger processes. In particular, in defective SQW, the defect-assisted Auger recombination rate can exceed the radiative one. Our results further suggest that the defect-assisted Auger recombination is expected to be all the more critical in green to red III-nitride light-emitting diodes due to their reduced radiative rate.

Despite the massive success of blue light-emitting diodes (LEDs) based on InGaN/GaN quantum wells (QWs), the internal quantum efficiency (IQE) of such LEDs is known to drop dramatically when increasing the current density above a few amperes per square centimeter, which is commonly denoted as "*efficiency droop*".[1–3] Auger recombination is one of the widely accepted mechanisms responsible for the droop observed in III-nitride (III-N) LEDs, which has been substantiated by experimental results.[4,5] Nevertheless, in wide direct band gap semiconductors, the direct band-to-band Auger process is expected to be weak, on the order of 10^{-34} cm^{6}s^{-1}, which is related to the strict conditions for conserving momentum and energy between initial and final states. Interestingly, however, the weight of indirect Auger processes is expected, in theory, to be comparatively larger than the direct one. Indeed, indirect processes can be mediated by carrier scattering mechanisms for which the constraint on the momentum and energy conservation rule is relaxed.[6–8] Besides, recent experimental studies provided evidence that, at cryogenic temperature, the indirect Auger process can be dramatically enhanced for localized carriers experiencing alloy disorder inherent to InGaN/GaN QWs.[9,10] Furthermore, some recent reports indicate that point defects (PDs) present in III-N materials, apart from being involved in the conventional Shockley-Read-Hall (SRH) recombination process, likely act as efficient scattering centers responsible for the indirect Auger process.[11–14] However, the relation existing between SRH and defect-assisted Auger processes is not fully understood yet, partly due to the lack of clear correlation between the PD density in the active layer and the respective weight of the SRH and Auger terms. Hence, experimental evidence and quantification of those terms are further required to evaluate the eventual impact of PDs on the carrier dynamics in the droop regime.

Earlier reports indicated that the density of nonradiative defects present in InGaN/GaN QWs can be drastically decreased if a thick InGaN layer, hereafter an underlayer (UL), is deposited before the growth of the active region.[15,16] As recently demonstrated, the PD density in the active QW region can be precisely controlled by playing with the indium content and the thickness of the UL as the latter two parameters determine the ability to trap surface defects (SDs) in the UL that could otherwise act as nonradiative centers if incorporated in the active medium.[17,18] Indium atoms playing an essential role in trapping SDs, InAlN nearly lattice-matched (LM) to GaN was successfully used as efficient UL.[19]

In this Letter, we build upon those previous works to tune the defect density in InGaN/GaN single QW (SQW) samples through a change in the thickness of a LM InAlN UL and evaluate its impact on Auger recombination using picosecond time-resolved photoluminescence (TR-PL) measurements at 300 K. The reported results are analyzed in the framework of a modified ABC model, which includes defect-assisted Auger recombination.

Three samples were grown by metalorganic vapor phase epitaxy, which share the same InGaN/GaN SQW with ∼12% In content and a width of 2.7 nm as in our previous work,[18] but have different $In_{0.15}Al_{0.85}N$ UL thicknesses of 0, 10 and 55 nm (See Sec. A of the supplementary material (SM) for details). First, we performed micro-PL and TR-PL measurements at 300 K as a function of laser fluence from low carrier density to the degenerate regime ($n > 10^{12}$ cm^{-2}) (See SM Sec. B).

Figure 1(a) presents time-integrated PL spectra of the three samples recorded at 0.6 μJ/cm^2, corresponding to the intermediate injection regime. The peak PL intensity (I_{PL}) of the QW luminescence is enhanced by more than two orders of magnitude as the InAlN UL thickness

a) Current address: Univ. Grenoble Alpes, CNRS, Grenoble INP, Institut Néel, 38000 Grenoble, France
b) Electronic mail: raphael.butte@epfl.ch

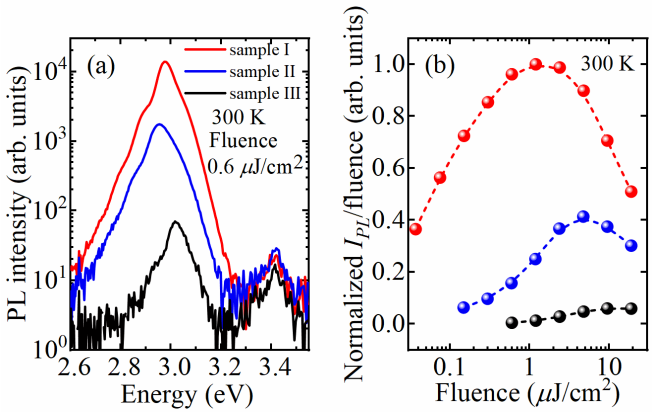

FIG. 1. (a) Time-integrated PL spectrum of sample-I, -II, and -III with an InAlN UL thickness of 55, 10 and 0 nm, respectively, measured at a fluence of 0.6 μJ/cm^2 and 300 K. (b) Normalized ratios of QW I_{PL} to fluence for those three samples, which corresponds to their relative PL efficiencies.

increases from 0 to 55 nm, which indicates a significant change in the defect density in the QW through the variation of the UL thickness. Figure 1(b) shows the evolution of the normalized ratios of QW I_{PL} to the fluence for the three investigated samples, which corresponds to the relative PL efficiency. The fluence at maximum PL efficiency for sample-I and -II shifts from ∼1 to 5 μJ/cm^2. Such a behavior is in line with the fact that as the defect concentration in SQW increases, the Auger recombination channel, which emerges under high injection, requires a larger carrier density to exceed the SRH one. Nevertheless, both samples exhibit a decrease in PL efficiency at high fluence, i.e., the well-known manifestation of efficiency droop.[12] For comparison, the PL efficiency of sample-III, without UL, only shows a monotonically increasing behavior, which indicates the dominant weight of SRH recombination in this latter case.

Figures 2(a)-2(c) show the fluence-dependent SQW integrated PL intensity decays for sample-I, -II and -III, respectively. Due to the increasing weight of SRH recombination, the decay time of sample-II, extracted from the monoexponential fit of the PL intensity decays recorded at low fluence, amounts to ∼2 ns compared to about 20 ns for sample-I. However, sample-I and -II both present a long monoexponential decay up to intermediate fluences, while for high fluences ($>$ 0.6 μJ/cm^2) fast non-exponential features occur at early delays. In line with the drop in PL efficiency observed at high fluence, those fast non-exponential decays indicate the presence of extra carrier losses, which results in the droop. On the other hand, the high defect density characteristic of sample-III leads to nearly monoexponential traces with extremely short decay times, around ∼50 ps.

Figures 2(d)-2(f) display the corresponding time-dependent evolutions of SQW PL spectra for the three samples from a fluence of 19 μJ/cm^2. They all exhibit a redshift of their QW emission spectra with increasing

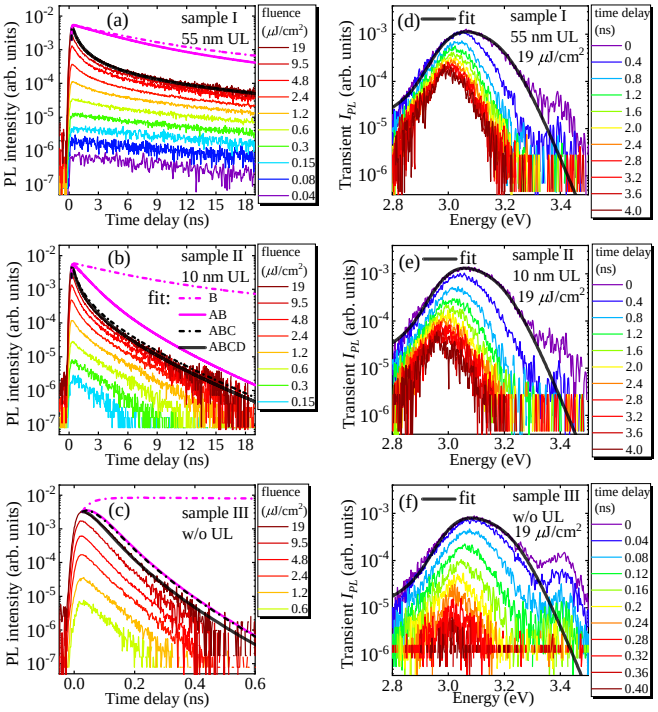

FIG. 2. (a) to (c): 300 K fluence-dependent SQW integrated PL intensity decays of sample-I, -II, and -III, respectively. The simulated decays only considering radiative recombination are shown as pink dash-dotted traces, labeled as B. The pink solid lines stand for the dynamics including radiative and SRH recombinations, labeled as AB whereas the black dash-dotted lines are the fits with contribution of the radiative, SRH and band-to-band Auger recombinations, labeled as ABC. Finally, the black solid lines correspond to the fits taking into account the radiative, SRH, band-to-band and defect-assisted Auger recombinations, labeled as ABCD. (d) to (f): Corresponding time-dependent spectral evolutions of sample-I, -II and -III. The black curves are the fits used to extract the carrier density based on Fermi's golden rule, which is estimated to be equal to 1.4×10^{13} cm^{-2} at a fluence of 19 μJ/cm^2 for sample-I and -II, and 1.5×10^{13} cm^{-2} for sample-III.

time delay, which is mainly related to the descreening of the built-in electric field. Furthermore, the asymmetric broadening of QW emission spectra toward bulk GaN emission at early delays suggests that the QW samples lie in the degenerate regime when subjected to such an initial carrier density, while the subsequent linewidth narrowing is linked to the decrease in the injected carrier density.[20]

To study the impact of PDs on the Auger recombination process in the droop regime, we quantify the carrier dynamics based on a modified ABC model taking into account defect-assisted Auger recombination. We first extract the initial carrier density by fitting the initial SQW emission lineshape under 19 μJ/cm^2 fluence based on Fermi's golden rule.[20,21] The fitting results are displayed as black lines in Figs. 2(d)-2(f), which well repro-

duce the Fermi filling induced broadening of QW emission, and give the initial carrier density of 1.4×10^{13} cm^{-2} for sample-I and -II, and 1.5×10^{13} cm^{-2} for sample-III. Subsequently, we simulate the change in the wave function overlap as a function of carrier density using the self-consistent Schrödinger-Poisson method in order to account for the progressive descreening of the built-in electric field with decreasing carrier density (detailed in SM Sec. C).

Next, we compare our experimental results with a modified ABC model:

$$\frac{dn}{dt} = -An - Bn^2 - Cn^3 - Dn^2, \tag{1}$$

where the four terms on the right-hand side of Eq. (1) account for the SRH, bimolecular, standard Auger, and defect-assisted Auger recombination, respectively.

First, in order to evaluate the impact of the built-in electric field screening on SRH recombination, we use a phenomenological formula that was recently proposed by A. David *et al.*:[12,22]

$$An = osc^p \cdot A_0 n, \tag{2}$$

where the exponent p accounts for the dependence of the SRH recombination rate on wave function overlap, and A_0 is the SRH coefficient in the low injection regime.

Second, the bimolecular recombination rate is expressed as:

$$Bn^2 = osc \cdot \int_{E_{QW}}^{\infty} R_{sp}(n,E)dE, \tag{3}$$

where $R_{sp}(n,E)$ is the spontaneous emission rate described by Fermi's golden rule,[20,21] which captures the phase-space filling effect in the degenerate regime from the QW ground state energy E_{QW}, while the prefactor osc accounts for the screening/descreening of the built-in field. We note that a recent study suggests that, in the low carrier density regime ($\leq$ a few 10^{11} cm^{-2}), Coulomb interaction can significantly enhance the radiative rate even at room temperature.[23] Since we mostly focus on recombination dynamics in the degenerate regime, i.e., under high injection, Coulomb interaction may be neglected in our model.

Third, in the three-particle Auger process the interband transition of e-h pairs is also subjected to screening/descreening and phase-space filling,[24] in a way equivalent to radiative recombination. For the sake of simplicity, while preserving its physical meaning, we assume that in the Auger process the energy issued from the nonradiative bimolecular-like recombination of an e-h pair is transfered to a third particle:

$$Cn^3 = C_0 \cdot n \cdot Bn^2, \tag{4}$$

where C_0 phenomenologically accounts for the Coulomb interaction between the third particle and the e-h pair, which also depends on energy and momentum conversation.

Theoretically, the defect-assisted Auger process is expected to become significant as defect density increases, due to carrier scattering mediated by defects.[25] As reported by David *et al.*,[12] the rate of defect-assisted Auger transitions exhibits an n^3 dependence in the low to intermediate carrier density regime for thick InGaN/GaN QWs grown on c-plane bulk GaN substrates (well width of 4 nm and In content ranging from 8 to 25%), which suggests that the defect levels act as virtual scattering states, i.e., without any carrier population build-up. On the other hand, it was reported that, in a well-established material such as silicon but also in monolayer MoS_2 and recently in low-IQE ($\leq$ 1%) III-N LEDs grown by molecular beam epitaxy, defects can act as effective scattering centers involving the capture of a free carrier that subsequently excites a second free carrier during the process.[13,26,27] Since the A coefficient contains information about the defect density and their average capture cross section, the defect-assisted Auger process is supposed to be intrinsically linked to SRH recombination. To further examine this scenario, we express the defect-assisted Auger rate as:

$$Dn^2 = k_D \cdot An^2, \tag{5}$$

where k_D is a proportionality coefficient that depends on the interaction between the first carrier captured by a given defect and the second free carrier (See also SM Sec. D).

We extract the related A, B, C and D coefficients by applying this model to simulate the PL decays recorded at high fluence (19 μJ/cm^2), i.e., in a regime that exceeds the range of carrier densities considered by David *et al.*[12] We first decompose the SRH and radiative recombination channels in sample-I by matching the PL decay at long delays and then derive an $\sim$20% maximum IQE.[19] The standard Auger coefficient can be subsequently determined by fitting the nonexponential decay at early delays. The radiative recombination coefficient has been kept identical for the three samples since they share the same QW structure. The same holds true for the standard Auger recombination process. For the more defective sample-II and -III, we notice a discrepancy between the measured PL decays and the modeling when the sole standard Auger recombination process is considered. Modeling and experimental results can be reconciled when adding the defect-assisted Auger recombination term. As shown in Figs. 2(a)-2(c), the pink dash-dotted lines illustrate the decay fits including only radiative recombination, labeled as B. The pink solid lines are the decays containing radiative and SRH recombination channels, labeled as AB, which govern the PL decays at longer delays. The black dash-dotted curves represent the contributions of radiative, SRH and standard Auger

recombination channels, labeled as ABC. In addition to those conventional channels, the black curves correspond to the fits taking into account the defect-assisted Auger channel, labeled as $ABCD$, which well reproduce the entire dataset. In sample I, the ABC and $ABCD$ curves almost perfectly overlap with each other, which suggests a marginal impact of defect-assisted Auger recombination in this latter case. However, as the point defect density increases, the difference between the ABC and $ABCD$ curves becomes more and more blatant as seen for sample-II and -III.

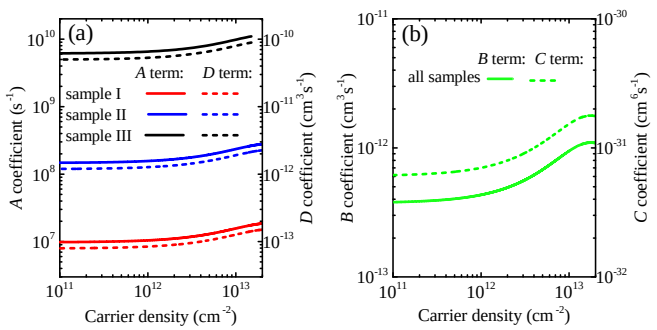

FIG. 3. (a) Carrier density dependent A and D coefficients, (b) B and C coefficients extracted, in the framework of the $ABCD$ model, from the fitting of PL decays at a fluence of 19 μJ/cm^2. Those values are issued from the data shown in Figs. 2(a) to 2(c).

Figure 3 displays the density dependent value of the A, B, C and D coefficients obtained after measuring each sample at different positions. As illustrated in Fig. 3(a), the A coefficient is reduced by more than two orders of magnitude when switching from sample-III to -I, as the PD density in the QW is reduced by the increase in UL thickness. Let us note that the A coefficient is marginally impacted by carrier density, due to its weak dependence on screening with $p = 0.35$ in our samples. This can be understood by the relatively thin QW thickness of 2.7 nm. As shown in Fig. 3(b), the B coefficient remains constant at $\sim 4\times10^{-13}$ cm^{3}s^{-1} below a carrier density of 5×10^{11} cm^{-2}, and then increases by a factor of two when n reaches 10^{13} cm^{-2}. The smaller enhancement of the B term compared to the density dependent $\langle\Psi|\Psi\rangle^2$ term is related to phase-space filling that takes place in the degenerate regime. Indeed, it leads to a reduction in the B coefficient because of the transition from a bimolecular to a monomolecular recombination process in the degenerate regime.[28] Those two joint effects also lead to a carrier density dependent C coefficient, which varies from 6×10^{-32} cm^6 s^{-1} to 2×10^{-31} cm^6 s^{-1} when n increases from 10^{11} cm^{-2} to 2×10^{13} cm^{-2}. Figure 3(a) reveals that the D coefficient varies from 10^{-13} cm^3 s^{-1} to 10^{-10} cm^{3}s^{-1} when switching from sample-I to -III. As shown in Fig. 4, the linear correlation between A and D coefficients leads to a scaling factor $k_D = 8\times10^{-21}$ cm^3. More importantly, the derived D value has the same magnitude as the B coefficient or even a larger one, which indicates a close competition between radiative and defect-assisted Auger processes. It is worth mentioning that this defect-assisted Auger process is expected to be less sensitive to screening effects because the two free carriers at play have the same charge, i.e., it involves either e-e or h-h pairs.[27] Consequently, the defect-assisted Auger process should be a critical carrier loss channel in green and red III-N LEDs, for which the B coefficient is significantly altered by the quantum confined Stark effect (QCSE).

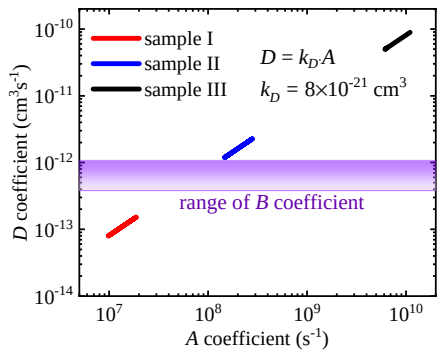

FIG. 4. Linear correlation extracted between A and D coefficients. Each segment illustrates the change in the value of the A and D coefficients, which are a function of carrier density (cf. Fig. 3(a)).

To conclude, we have studied the impact of PDs on the Auger recombination mechanism in c-plane InGaN/GaN QWs in the droop regime by tuning the defect density in the active layer by varying the thickness of an InAlN UL. Through high injection TR-PL measurements and modeling of the PL decays, we showed that, besides SRH and standard Auger recombination, including an additional defect-assisted Auger process –where SRH-type defects act as scattering centers– is necessary to reconcile the discrepancy observed between the usual ABC model and experimental observations. We examined the scenario of point defects acting as actual trap states, where the rate of defect-assisted Auger process is proportional to n^2. Our results indicate a linear dependence between the SRH coefficient A and the defect-assisted Auger coefficient D, which scales as $D = k_D \cdot A$ with $k_D = 8 \times 10^{-21}$ cm^3. They also evidence that the weight of the A term can lead to D values exceeding the value of the bimolecular recombination coefficient B. Our work further suggests that the defect-assisted Auger recombination channel should be a critical carrier loss mechanism in green and red III-N LEDs, which are plagued by a low B term stemming from the detrimental impact of the QCSE. Combined with the recently reported defect-assisted Auger rate via a virtual scattering state, which scales like n^3,[12] our study shows that a dual scattering mechanism via defects is likely at play, whose exact weight will depend on the carrier density, defect density, and QW geometry. This work will obviously call

for additional studies on the exact scattering mechanism at play in the defect-assisted Auger process.

See supplementary material for a description of (A) the sample structure, (B) experimental details on TR-PL, (C) the modeling of the carrier density dependent QCSE by the self-consistent Schrödinger-Poisson method, (D) the correlation between A and C coefficients, and (E) the link between carrier density, current density and IQE.

The data that support the findings of this study are available from the corresponding author upon reasonable request.

ACKNOWLEDGMENTS

This work was supported by the Swiss National Science Foundation through Grants No. 200020_182442 and 200020E_175652.

[1] J. Cho, E. F. Schubert, and J. K. Kim, Laser & Photonics Reviews **7**, 408 (2013).
[2] M. R. Krames, G. Christenson, D. Collins, L. W. Cook, M. G. Craford, A. Edwards, R. M. Fletcher, N. F. Gardner, W. K. Goetz, W. R. Imler, *et al.*, in *Light-Emitting Diodes: Research, Manufacturing, and Applications IV*, Vol. 3938, edited by H. W. Yao, I. T. Ferguson, and E. F. Schubert (International Society for Optics and Photonics, 2000) pp. 2–12.
[3] T. Mukai, M. Yamada, and S. Nakamura, Japanese Journal of Applied Physics **38**, 3976 (1999).
[4] J. Iveland, L. Martinelli, J. Peretti, J. S. Speck, and C. Weisbuch, Physical Review Letters **110**, 177406 (2013).
[5] M. Binder, A. Nirschl, R. Zeisel, T. Hager, H.-J. Lugauer, M. Sabathil, D. Bougeard, J. Wagner, and B. Galler, Applied Physics Letters **103**, 071108 (2013).
[6] E. Kioupakis, P. Rinke, K. T. Delaney, and C. G. Van de Walle, Applied Physics Letters **98**, 161107 (2011).
[7] F. Bertazzi, X. Zhou, M. Goano, G. Ghione, and E. Bellotti, Applied Physics Letters **103**, 081106 (2013).
[8] E. Kioupakis, D. Steiauf, P. Rinke, K. T. Delaney, and C. G. Van de Walle, Phys. Rev. B **92**, 035207 (2015).
[9] M. Shahmohammadi, W. Liu, G. Rossbach, L. Lahourcade, A. Dussaigne, C. Bougerol, R. Butté, N. Grandjean, B. Deveaud, and G. Jacopin, Physical Review B **95**, 125314 (2017).
[10] W. Liu, G. Rossbach, A. Avramescu, T. Schimpke, H.-J. Lugauer, M. Strassburg, C. Mounir, U. Schwarz, B. Deveaud, and G. Jacopin, Physical Review B **100**, 235301 (2019).
[11] A. David, N. G. Young, C. Lund, and M. D. Craven, ECS Journal of Solid State Science and Technology **9**, 016021 (2020).
[12] A. David, N. G. Young, C. A. Hurni, and M. D. Craven, Physical Review Applied **11**, 031001 (2019).
[13] A. C. Espenlaub, D. J. Myers, E. C. Young, S. Marcinkevičius, C. Weisbuch, and J. S. Speck, Journal of Applied Physics **126**, 184502 (2019).
[14] D. J. Myers, K. Gelžinytė, A. I. Alhassan, L. Martinelli, J. Peretti, S. Nakamura, C. Weisbuch, and J. S. Speck, Physical Review B **100**, 125303 (2019).
[15] T. Akasaka, H. Gotoh, T. Saito, and T. Makimoto, Applied Physics Letters **85**, 3089 (2004).
[16] A. M. Armstrong, B. N. Bryant, M. H. Crawford, D. D. Koleske, S. R. Lee, and J. J. Wierer Jr., Journal of Applied Physics **117**, 134501 (2015).
[17] C. Haller, J.-F. Carlin, G. Jacopin, D. Martin, R. Butté, and N. Grandjean, Applied Physics Letters **111**, 262101 (2017).
[18] C. Haller, J.-F. Carlin, G. Jacopin, W. Liu, D. Martin, R. Butté, and N. Grandjean, Applied Physics Letters **113**, 111106 (2018).
[19] C. Haller, J.-F. Carlin, M. Mosca, M. D. Rossell, R. Erni, and N. Grandjean, Applied Physics Express **12**, 034002 (2019).
[20] G. Rossbach, J. Levrat, G. Jacopin, M. Shahmohammadi, J.-F. Carlin, J.-D. Ganière, R. Butté, B. Deveaud, and N. Grandjean, Physical Review B **90**, 201308(R) (2014).
[21] M. Shahmohammadi, G. Jacopin, G. Rossbach, J. Levrat, E. Feltin, J.-F. Carlin, J.-D. Ganière, R. Butté, N. Grandjean, and B. Deveaud, Nature Communications **5**, 5251 (2014).
[22] A. David, C. A. Hurni, N. G. Young, and M. D. Craven, Applied Physics Letters **111**, 233501 (2017).
[23] A. David, N. G. Young, and M. D. Craven, Physical Review Applied **12**, 044059 (2019).
[24] A. David and M. J. Grundmann, Applied Physics Letters **96**, 103504 (2010).
[25] D. J. Robbins and P. T. Landsberg, Journal of Physics C: Solid State Physics **13**, 2425 (1980).
[26] S. K. Pang, A. W. Smith, and A. Rohatgi, IEEE Transactions on Electron Devices **42**, 662 (1995).
[27] H. Wang, C. Zhang, and F. Rana, Nano Letters **15**, 339 (2015).
[28] W. Liu, R. Butté, A. Dussaigne, N. Grandjean, B. Deveaud, and G. Jacopin, Phys. Rev. B **94**, 195411 (2016).
[29] A. David, C. A. Hurni, N. G. Young, and M. D. Craven, Applied Physics Letters **109**, 083501 (2016).
[30] D. Kleinman and R. Miller, Physical Review B **32**, 2266 (1985).
[31] M. Yoshikawa, M. Kunzer, J. Wagner, H. Obloh, P. Schlotter, R. Schmidt, N. Herres, and U. Kaufmann, Journal of Applied Physics **86**, 4400 (1999).